Controlling Reversible Expansion of Li_2O_2 Formation and Decomposition by Modifying Electrolyte in Li-O_2 Batteries

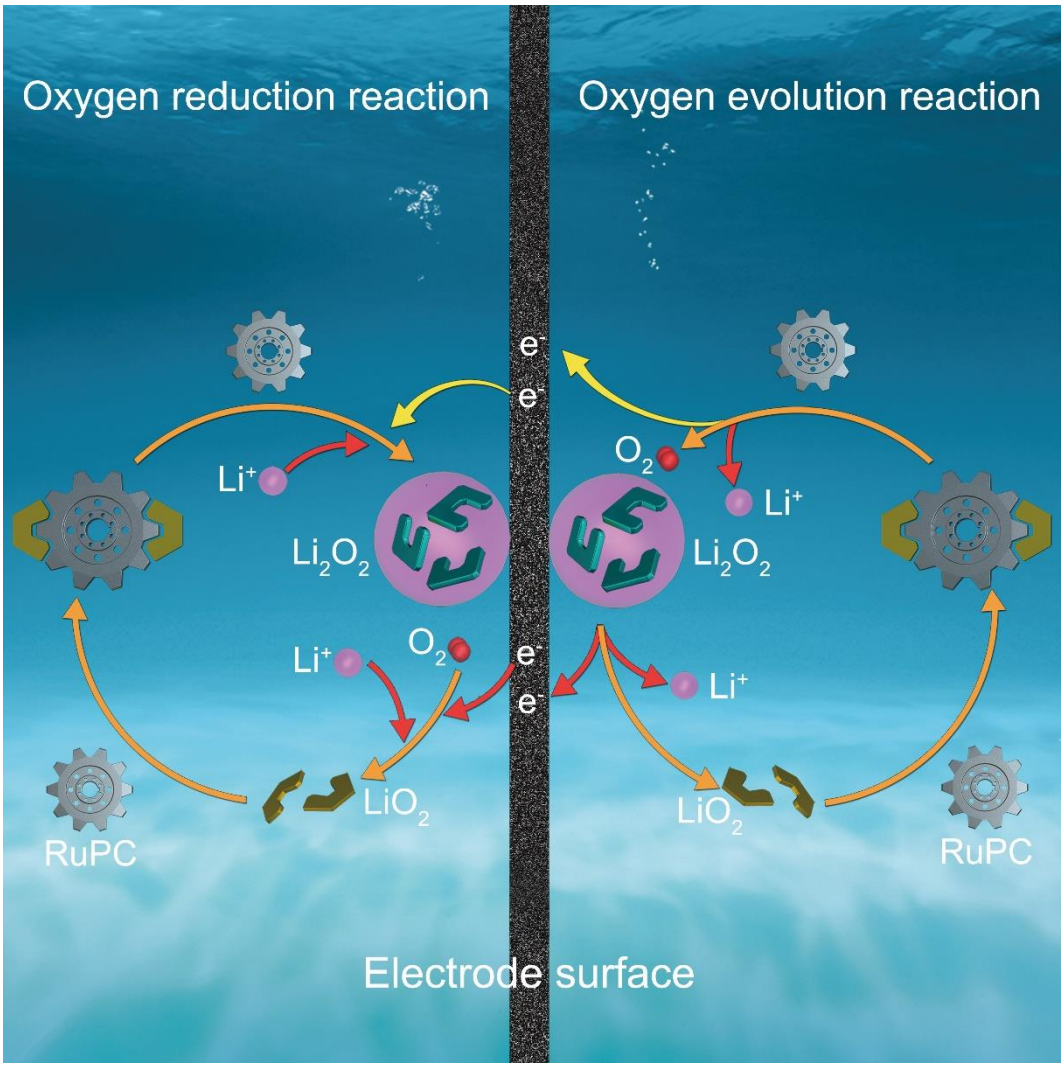

The development of the Li-O_2 battery is critically hindered by cathode passivation, large polarization, and severe parasitic reactions. Here, Dong and co-workers employ a Ru(II) polypyridyl complex (RuPC) as a multifunctional soluble electrocatalyst for Li-O_2 batteries to address these issues. Benefiting from the interaction between the Ru(II) center and O_2^-/LiO_2 species, the RuPC can not only reversibly expand Li_2O_2 formation and decomposition with a low overpotential but also limit the side reactions. As a result, the RuPC-catalyzed Li-O_2 batteries exhibit excellent performance.

Controlling Reversible Expansion of Li_2O_2 Formation and Decomposition by Modifying Electrolyte in Li-O_2 Batteries

Xiaodong Lin,[1,3] Ruming Yuan,[1,3] Yong Cao,[2] Xiaobing Ding,[1] Senrong Cai,[1] Bowen Han,[1] Yuhao Hong,[1] Zhiyou Zhou,[1] Xulai Yang,[2] Lei Gong,[1]* Mingsen Zheng,[1]* and Quanfeng Dong[1,4]*

[1]Collaborative Innovation Center of Chemistry for Energy Materials (*i*ChEM), State Key Laboratory of Physical Chemistry of Solid Surfaces, Department of Chemistry, College of Chemistry and Chemical Engineering, Xiamen University, Xiamen, Fujian 361005, China

[2]Hefei Guoxuan High-tech Power Energy Co., Ltd., Hefei, Anhui 230011, China

[3]These authors contributed equally

[4]Lead Contact

*Correspondence: qfdong@xmu.edu.cn (Q.D.), mszheng@xmu.edu.cn (M.Z.), gongl@xmu.edu.cn (L.G.)

Summary

The aprotic lithium-oxygen (Li-O_2) battery has attracted worldwide attention because of its ultrahigh theoretical energy density. However, its practical application is critically hindered by cathode passivation, large polarization, and severe parasitic reactions. Here, we demonstrate an originally designed Ru(II) polypyridyl complex (RuPC) though which the reversible expansion of Li_2O_2 formation and decomposition can be achieved in Li-O_2 batteries. Experimental and theoretical results revealed that the RuPC can not only expand the formation of Li_2O_2 in electrolyte but also suppress the reactivity of LiO_2 intermediate during discharge, thus alleviating the cathode passivation and parasitic reactions significantly. In addition, an initial delithiation pathway can be achieved when charging in turn; thus, the Li_2O_2 products can be

decomposed reversibly with a low overpotential. Consequently, the RuPC-catalyzed Li-O_2 batteries exhibited a high discharge capacity, a low charge overpotential, and an ultralong cycle life. This work provides an alternative way of designing the soluble organic catalysts for metal-O_2 batteries.

Keywords

lithium-oxygen battery; cathode passivation; large polarization; severe parasitic reactions; Ru(II) polypyridyl complex; multifunctional soluble catalyst; initial delithiation pathway; high discharge capacity; low charge overpotential; ultralong cycle life

Introduction

Because of the increasing demands for portable devices and light vehicles, new energy storage systems with high energy densities have been widely investigated.[1-4] Among them, the rechargeable aprotic lithium-oxygen (Li-O_2) battery has attracted tremendous attention because its theoretical energy density is about ten times that of the state-of-the-art Li-ion battery.[5-8] However, the development of current Li-O_2 battery is critically hindered by limited capacity (far less than theory), low energy efficiency and poor cycle life,[9-13] which can be attributed to the electrical passivation of the cathode surface by the insulated Li_2O_2,[14,15] poor Li_2O_2/catalyst contact interface[16,17] and undesired side reactions.[18,19]

In the past few years, after a lot of systematic studies, many researchers have reached a consensus that growth of Li_2O_2 thin films on the cathode surface would severely passivate the O_2 cathode and thus lead to low discharge capacity and premature battery death, whereas inducing Li_2O_2 to grow in the electrolyte could avoid cathode passivation and achieve high

discharge capacity and improved cycle life.[20-28] Hence, many groups have recently tried various ways to promote the solution mechanism to realize the effective growth of Li_2O_2 in the electrolyte.[14,23-28] Viswanathan and coworkers disclosed that trace amounts of high-acceptor-number additive, such as water or methanol, could promote the solution-phase growth of Li_2O_2 in electrolyte.[14] Bruce and coworkers reported that the addition of 2,5-di-tert-butyl-1,4-benzoquinone (DBBQ) to low-donor-number solvents could also induce Li_2O_2 to grow in electrolyte.[23] Peng's group selected a biomolecule (coenzyme Q_{10}) as a soluble catalyst for Li-O_2 batteries to trigger solution-phase formation of Li_2O_2 in ether-based electrolyte,[24] whereas Nakanishi and coworkers used potassium ions to prompt a solution route of Li_2O_2 formation.[25] Although these works have greatly improved the electrical passivation of the cathode surface during the discharge process and greatly increased the discharge capacity, large overpotential and severe irreversibility still exist in the charge process of these batteries.

Some recent studies have also disclosed that growth of Li_2O_2 in the electrolyte would cause a poor Li_2O_2/cathode contact interface, which could impede the full play of the catalytic activity on charge, leading to large overpotential and even the incomplete decomposition of Li_2O_2 in charge process.[2,23-25,29,30] Moreover, the formation of Li_2O_2 in the electrolyte would also aggravate the side reactions because its intermediates, LiO_2 and O_2^-, readily attack the electrolyte solvents, resulting in poor reversibility.[19,31-36] On the basis of the above analysis, one of the most challenging issues in current Li-O_2 batteries is how to reversibly expand Li_2O_2 formation and decomposition with a low overpotential.

We present a Ru(II) polypyridyl complex (RuPC) as a multifunctional soluble electrocatalyst for both discharge and charge processes of the Li-O_2 battery, where the Ru center can interact

with the LiO_2 intermediate and induce it to dissolve into electrolyte, thus expanding the formation of Li_2O_2 in electrolyte and alleviating the cathode passivation significantly during discharge, and the interface between catalyst and product has also been improved significantly. When charging in turn, the interaction between the Ru center and the LiO_2 intermediate can also promote the initial delithiation of Li_2O_2 products, which is a more kinetically favorable and highly reversible pathway. Moreover, because of the interaction between the Ru center and the LiO_2 intermediate, the RuPC catalyst can serve as a highly mobile trap for the LiO_2 intermediate to suppress the superoxide-related parasitic reactions, thus increasing the reversibility of the Li-O_2 battery. As a result, the RuPC-catalyzed Li-O_2 batteries can deliver a high discharge capacity (~9281 mAh g^{-1}) that is two to three times what the RuPC-free ones (~4100 mAh g^{-1}) can achieve, an ultralong cycle life (371 cycles) that is ~31 times what the RuPC-free ones can achieve (12 cycles), and a lower charge overpotential (0.54 V) than that of the RuPC-free ones (1.30 V), as well as reduced side products. Finally, we have revealed the O_2 redox mechanisms of the RuPC-catalyzed Li-O_2 batteries by combining the experimental and theoretical results.

Results and discussion

To reversibly expand Li_2O_2 formation and decomposition with a low overpotential, several key conditions need to be satisfied: (1) the ability to induce LiO_2 to dissolve into the electrolyte, (2) the power to suppress the high reactivity of LiO_2, and (3) good Li_2O_2/catalyst contact interface. It is well known that O_2^- has a relatively large radius and low charge density and can be considered as a moderately soft base.[37] On the basis of the hard-soft acid-base theory, a substance with the properties of soft acid can interact with O_2^- species and control its reactivity.

In addition, the removable solution-phase catalyst can reach everywhere in the electrolyte and provide a good Li_2O_2/catalyst contact interface. Thus, taking the above conditions into account, the metal-organic complexes are the primary choice because they have superior catalytic activities and high solubility in organic solvents.[38-40] Moreover, the metal center that has unoccupied orbitals in metal-organic complex can be regarded as Lewis acid, and most of them have the properties of soft acids that can interact with LiO_2 intermediate, thus inducing LiO_2 to dissolve into the electrolyte and suppressing the reactivity of LiO_2.[40] To verify these concepts, we synthesized a RuPC (compound **2**) through the reaction of *cis*-$Ru(bpy)_2Cl_2 \cdot 2H_2O$ with a thioether-containing oxazoline (compound **1**) (see Experimental Procedures and Figures 1A and S1),[41,42] and then used it as a multifunctional soluble catalyst for Li-O_2 batteries. As shown in Figures S2-S5, the structure of RuPC was well-established by the ^1H nuclear magnetic resonance (NMR), ^{13}C-NMR, Fourier transform infrared (FTIR), and high-resolution mass spectrometry (HRMS) spectra.

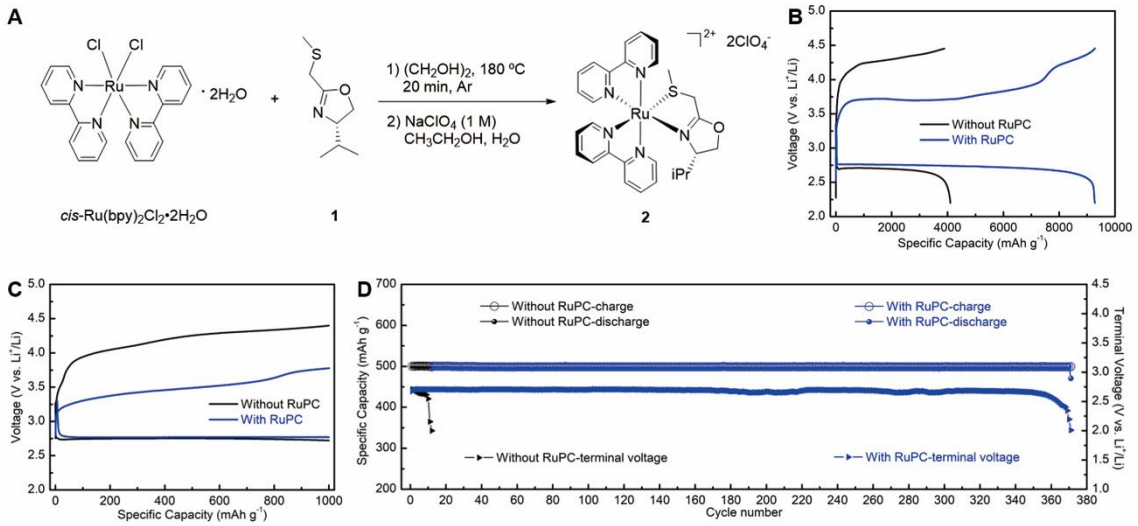

Figure 1. The Synthetic Route of RuPC and Electrochemical Performance of Li-O_2 Batteries

(A) The synthetic route of RuPC, compound **2**. See also Figures S1-5.

(B) Full charge-discharge curves of Li-O_2 batteries with and without RuPC in a voltage window between 2.2 and 4.45 V at a current density of 200 mA g^{-1}.

(C) Voltage profiles of Li-O_2 batteries with and without RuPC at a current density of 100 mA g^{-1} with a cutoff capacity of 1000 mAh g^{-1}.

(D) Cycling stability and the terminal discharge voltage of Li-O_2 batteries with and without RuPC at a current density of 400 mA g^{-1} with a cutoff capacity of 500 mAh g^{-1}. See also Figure S10.

Next, to understand the electrochemical behavior of RuPC and to distinguish it from the redox mediators reported before,[16,17,43,44] we conducted a cyclic voltammetry (CV) experiment in a typical Li-O_2 battery environment (Figure S6). Under an argon atmosphere (Figure S6A), both curves of the Li-O_2 batteries with (red) and without (black) RuPC show no reaction features in the voltage range between 2.2 V and 4.2 V, whereas the one with RuPC exhibits the Ru^{2+}/Ru^{3+} redox couple in the potential of ~4.64 V. As a comparison, measurements in O_2 atmosphere were also carried out (Figure S6B). Both the batteries with (red) and without (black) RuPC exhibit a cathodic peak associated with oxygen reduction reaction (ORR) near 2.62 V; however, the cathodic peak current of the battery with RuPC is larger than that of the RuPC-free one, implying the RuPC can promote the ORR. Notably, a significant difference appears in the anodic region. The battery without RuPC shows a sharp anodic peak at ~4.44 V, which is attributed to Li_2O_2 decomposition and indicates the sluggish kinetics of the oxygen evolution reaction (OER), whereas the battery with RuPC exhibits a lower anodic peak at ~3.73 V. These observations demonstrate that the introduction of RuPC in the Li-O_2 battery could reduce the OER overpotential significantly. Distinctly, because the Li_2O_2 oxidation (~3.73 V) is prior to

the RuPC oxidation (~4.64 V) in RuPC-containing Li-O_2 batteries, the mechanism of the OER overpotential improvement in this case is different from that of redox mediators.[16,17,43,44] Hence, the RuPC does not act as a redox mediator here, and the OER overpotential improvement would be due to the catalytic activity of RuPC on Li_2O_2 decomposition.

To confirm that the improved electrochemical performances were caused by RuPC, we chose the carbon black nanoparticles as cathode material without loading any other catalysts. Figure 1B illustrates the full discharge curves of the Li-O_2 batteries with and without RuPC in a 0.5 M $LiClO_4$/DMSO system. The RuPC-catalyzed Li-O_2 batteries exhibited a high discharge capacity of ~9281 mAh g^{-1} at a current density of 200 mA g^{-1}, which is two to three times higher than that of the RuPC-free Li-O_2 batteries (~4100 mAh g^{-1}). To identify whether the capacity was derived from an O_2 reduction reaction, we discharged the battery with RuPC under Ar atmosphere. As shown in Figure S7, a negligible capacity of 2.7 mAh g^{-1} was observed, which means the discharge capacity of the RuPC-containing Li-O_2 battery was indeed contributed by the O_2 reduction. These outcomes demonstrate that the discharge capacity of the Li-O_2 battery could be significantly enhanced by RuPC, which is consistent with the results of CV experiment. As for the charge process, the charging overpotential of the Li-O_2 battery also obtained a significant improvement in the presence of RuPC (Figures 1B and 1C). Specifically, at a current density of 100 mA g^{-1} with a cutoff capacity of 1000 mAh g^{-1} (Figure 1C), the battery without RuPC exhibited a voltage platform at about 4.26 V in charge process, whereas that of the RuPC-containing battery was only 3.50 V; moreover, the lower charging voltage could be achieved with the increased RuPC concentration (Figure S8). According to the electrochemical impedance spectrometry (EIS) results (Figure S9 and Table S1), the overpotential reduction is

not due to the solution resistance decline. Therefore, such a significant improvement suggests that the kinetics of Li_2O_2 decomposition was promoted greatly by RuPC, confirming the catalytic role of RuPC. Furthermore, the Li-O_2 batteries with and without RuPC were tested at a current density of 400 mA g^{-1} with a cutoff capacity of 500 mAh g^{-1}. The charge voltage platforms of the battery with RuPC could still be maintained at around 3.75 V even after 300 cycles (Figure S10A), whereas that of the battery without RuPC soon increased to 4.0 V and then remained above 4.2 V (Figure S10B). In addition, the discharge terminal voltage of the battery without RuPC decreased to 2.0 V early at the 12^{th} cycle, and the discharge terminal voltage of the battery with RuPC remained above 2.0 V steadily even after 371 cycles (Figure 1D). Further, when under a cutoff capacity of 1000 mA h g^{-1}, the RuPC-containing Li-O_2 battery could still operate stably over 100 cycles at a current density of 400 mA g^{-1} (Figure S11). Besides, the RuPC-containing Li-O_2 batteries exhibited good rate capability with discharge capacities of ~11031, ~9281, and ~7723 mAh g^{-1} at current densities of 100, 200 and 300 mA g^{-1}, respectively (Figure S12). Moreover, the voltage attenuation of the discharge or charge process was not obvious as the current density increased. These outcomes fully supported that the electrochemical performance of the Li-O_2 battery could be significantly improved by RuPC.

Further, the discharged and charged carbon electrodes were extracted and detected by scanning electron microscope (SEM). In the absence of RuPC, the particles with toroidal morphology and the film-like discharge products were co-existing on the carbon surface after full discharge (Figures 2A, 2B, S13A, and S13B). However, when RuPC was present, only toroidal particles, clearly and compactly, could be found on the carbon surface after full discharge (Figures 2C, 2D, S13C and S13D). Such an observation also suggests intuitively that

the expanding formation of Li_2O_2 in electrolyte was achieved by RuPC during the discharge process. As for the charge process, although most of the discharge products have been decomposed, some cracked products derived from the toroidal particles could still be observed in the RuPC-free batteries (Figures 2E, 2F, and S14), implying the incomplete decomposition of the discharge products. Different from that of the RuPC-free batteries, the discharge products of the RuPC-containing batteries were completely removed (Figures 2G and 2H) after full charge and the surface morphology of the charged carbon electrode was almost the same as that of the pristine carbon electrode (Figure S15). In addition, even after cycling for 100 and 200 cycles (Figure S16), the cathode surfaces of the RuPC-containing Li-O_2 batteries were still almost the same as the pristine cathode surface (Figure S15). The SEM results demonstrate that the RuPC could expand the formation of Li_2O_2 in electrolyte and enhance the reversibility of Li-O_2 battery.

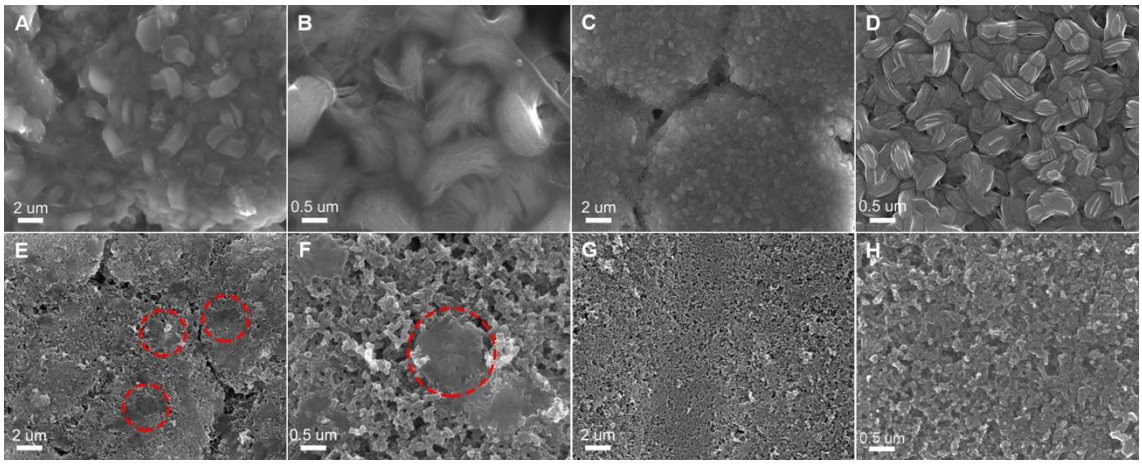

Figure 2. Morphologies of the Discharged and Charged Cathode Surface

SEM images showing the cathode morphologies of the Li-O_2 batteries after full discharge without (A and B) and with (C and D) RuPC, as well as after full charge without (E and F) and with (G and H) RuPC in a 0.5

M $LiClO_4$/DMSO system. The red dashed circles in (E) and (F) highlight the discharge product that cannot be decomposed completely after full charge without RuPC. See also Figures S13–S15.

To confirm that the products generated on the surface of the carbon electrode were indeed Li_2O_2, we monitored the carbon cathode by X-ray diffraction (XRD) technology. As shown in Figure 3A, the XRD pattern for the carbon cathode after discharge showed that the main discharge product was Li_2O_2, which is consistent with the reported literature.[23,26] After charge, the peaks of Li_2O_2 disappeared and the XRD pattern was the same as that of the pristine electrode before discharge. These outcomes revealed that the Li_2O_2 product was fully removed after charge, justifying the good reversible formation and decomposition of Li_2O_2 with RuPC. *Ex situ* X-ray photoelectron spectroscopy (XPS) characterization of the O_2 electrodes after discharge and charge were conducted as well (Figures 3B-3D). The C 1s XPS spectra of the pristine, discharged, and charged electrodes in the presence of RuPC all showed only five peaks centered at 284.5, 285.1, 286.1, 289.7, and 291.8 eV, assigned to C-C=C, -CH_2-CF_2-, C-O, O-C=O and -CH_2-CF_2- bonds,[45-47] respectively, and no other peaks were observed. In addition, the O 1s spectrum disclosed that Li_2O_2 was the only product of the discharged cathode in the presence of RuPC and it was decomposed completely after charge. This further established the good reversible formation and decomposition of Li_2O_2 with RuPC. On the contrary, the evidence of the Li_2CO_3 species in C 1s and O 1s spectra after discharge and charge without RuPC reveals that parasitic reactions existed during battery operation (Figure S17),[19,46,48] implying the incomplete decomposition of the discharge products and the inferior reversibility

of the battery without RuPC. The above outcomes demonstrated that the RuPC can suppress the side reactions effectively and enhance the reversibility of Li-O_2 batteries.

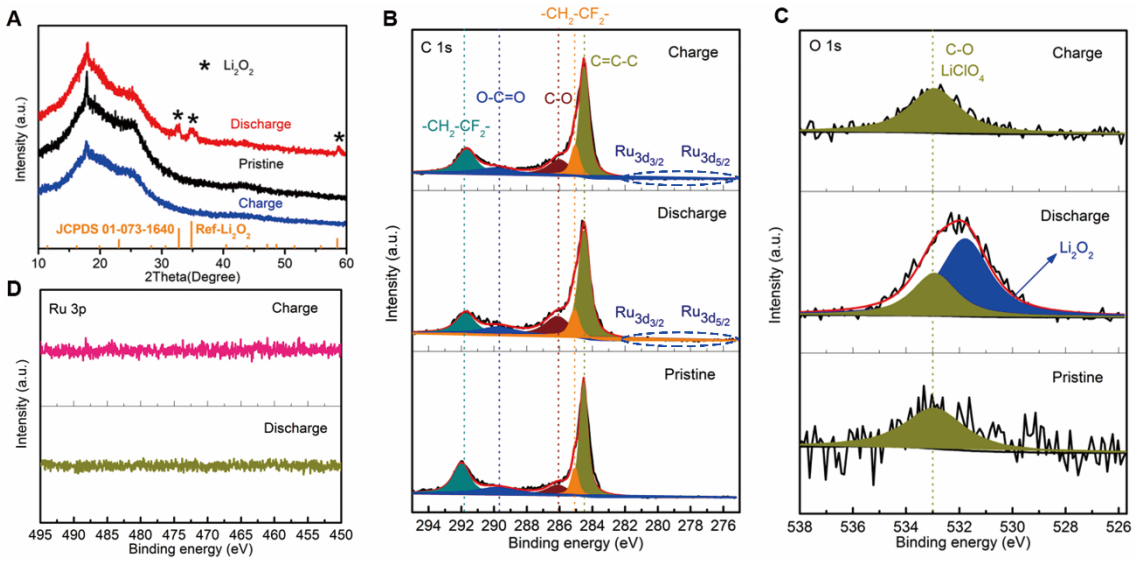

Figure 3. *Ex Situ* Spectral Characterizations of the Carbon Cathodes

(A) XRD patterns of the carbon cathodes extracted from the RuPC-catalyzed Li-O_2 batteries in pristine, discharged, and charged states.

(B–D) C 1s (B), O 1s (C), and Ru 3p (D) XPS spectra of the carbon cathodes extracted from the RuPC-catalyzed Li-O_2 batteries in pristine, discharged, and charged states. See also Figure S17.

To analyze the stability of RuPC during battery operation, we characterized the cathode, electrolyte and Li anode of the RuPC-containing Li-O_2 batteries. For the O_2 cathode, we compared the Ru 3d and 3p XPS regions of the discharged and charged electrodes to evaluate whether the RuPC decomposes during battery cycling. No peaks were associated with Ru species from the discharged and charged electrode (Figures 3B and 3D), suggesting the RuPC was stable and did not decompose in the cathode side during cycling. Li metal can react with a lot of organic species due to its lowest negative electrochemical potential. However, in Li

battery systems, the Li anode can react with the organic electrolyte solvent, Li salt, and electrolyte additive to form a so-called solid electrolyte interphase (SEI) layer during initial cycles, which can cover the Li anode surface, thus hindering further reactions of Li metal and organic species.[49-50] Hence, we used the XPS technology to analyze the surface composition of the Li anode to see whether the SEI layer would be stable after several cycles, thus preventing the further reaction of RuPC and Li metal. As shown in Figure S18, in the case of RuPC-containing Li-O_2 batteries, the SEI layer began to form during the first cycle, which contains Li_2CO_3, LiOH, Li_2SO_4, polythionate complex, thiosulphate, pyridinic N and the Ru-containing species, which might be assigned to Li_2RuO_3.[49,51-54] The S and O contents could be due to the reaction of the Li anode and DMSO solvent, and the N and Ru contents may be due to the reaction between Li and RuPC. Notably, all the spectra (C 1s, O 1s, N 1s and S 2p) of the 30th and 100th cycles were almost completely coincident, indicating the SEI layer was almost completely stable after 30 cycles and the reaction between Li and RuPC/DMSO had been prevented. That is also the critical factor in why the RuPC-containing Li-O_2 batteries can obtain very long cycles (~ 371 cycles). For comparison, the Li anodes of the RuPC-free batteries were also analyzed. Because of the short life (~ 12 cycles) of the RuPC-free batteries, we only tested the Li anodes after one, five, and ten cycles (Figure S19). Compared with the XPS results of the RuPC-containing Li-O_2 batteries, the SEI components of the Li anode in the RuPC-free Li-O_2 batteries contain Li_2CO_3, LiOH, Li_2SO_4. Moreover, after the initial ten cycles, the SEI layer has not yet achieved complete stability. The XPS results of the Li anode demonstrated that the RuPC is compatible with Li metal after forming a stable SEI layer on the Li anode surface, showing the feasibility of the application of RuPC in Li-O_2 batteries. Furthermore, the ^{1}H NMR

spectra of the RuPC-containing electrolyte after cycling has also confirmed the good stability of RuPC during reactions (Figure S20).

Further, gas evolution during the charge process has been monitored by differential electrochemical mass spectroscopy (DEMS), and the results are shown in Figure S21 and Table S2. As for the Li-O_2 battery without RuPC, there is a big gap between the detected O_2 evolution rate and the theoretical value ($2e^-/O_2$) during the charge process; moreover, the amount of CO_2 evolved is also very large. On the contrary, the detected O_2 evolution rate of the RuPC-contained Li-O_2 batteries is quite close to the $2e^-/O_2$ line and the amount of CO_2 evolved is relatively small. By integrating the O_2 evolution curve at different charge capacities and comparing with the corresponding theoretical amounts of O_2 evolved, we calculated the e^-/O_2 value for both the Li-O_2 batteries with and without RuPC. For the RuPC-free Li-O_2 battery, the values of e^-/O_2 are about ~3.49 at 0.05 mAh, ~3.84 at 0.1 mAh, ~3.38 at 0.15 mAh, ~2.94 at 0.2 mAh, and ~3.01 at 0.25 mAh, whereas for the RuPC-containing Li-O_2 battery, e^-/O_2 values of ~2.24 at 0.05 mAh, ~2.29 at 0.1 mAh, ~2.30 at 0.15 mAh, ~2.28 at 0.2 mAh, and ~2.44 at 0.25 mAh were obtained. In addition, the amount of CO_2 evolved in the RuPC-free battery is about 0.623 μmol, whereas that of the RuPC-containing battery is only about 0.267 μmol. These DEMS results have provided solid evidence for the reversibility of the O_2 redox reactions in the RuPC-containing Li-O_2 battery. Besides, the comparison of the DEMS results between the RuPC-free and -containing Li-O_2 batteries also indicated that the introduction of RuPC in the Li-O_2 battery system could not only reduce the charge overpotential but also suppress the related parasitic reactions and thus enhance the reversibility of Li-O_2 batteries.

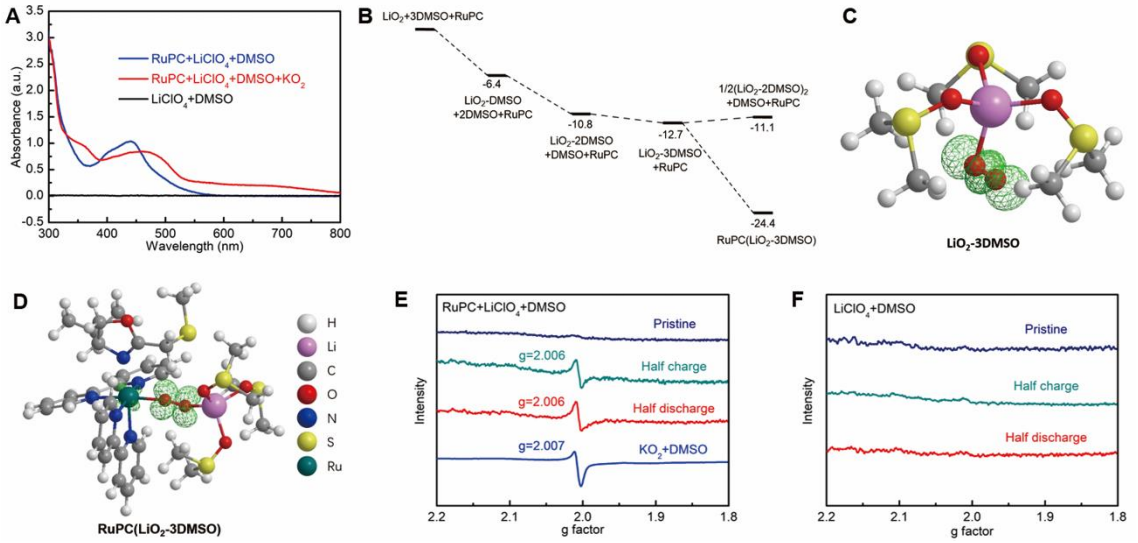

Figure 4. Interaction between RuPC and Superoxide Species

(A) The UV-vis spectrum of the $LiClO_4$/DMSO system with RuPC systems before and after the addition of KO_2 + DMSO solution.

(B) The free-energy profile of LiO_2 interacted with DMSO molecule(s) and RuPC. Binding free energies are given in kcal mol^{-1}. See also Figure S22.

(C and D) The optimized structure of LiO_2 interacted with (C) three DMSO molecules and (D) RuPC and three DMSO molecules (the green lobes represent the spin density isosurface at the isovalue of 0.05 $eÅ^{-3}$, and the bonds between LiO_2 and DMSO represent solvation effect). See also Figure S22.

(E and F) The EPR spectra of the KO_2 + DMSO solution and the electrolyte of Li-O_2 batteries (E) with and (F) without RuPC at pristine, half-discharged, and half-charged states. See also Figure S23.

To understand the reaction mechanisms of the RuPC-catalyzed Li-O_2 batteries, we conducted the UV-visible (UV-vis) absorption experiment and density functional theory (DFT) calculations to investigate the interaction between RuPC and O_2^- species. Figure 4A shows that, when the RuPC is introduced into the $LiClO_4$ + DMSO electrolyte, a broad peak appears at

about 440 nm, which can be attributed to the metal-to-ligand charge-transfer band.[55] Interestingly, the peak has a small red shift (change to 470 nm) after the addition of the KO_2 + DMSO solution, which can be attributed to the interaction between O_2^- species and RuPC.[16,48] We further performed DFT calculation to understand the interaction mechanism between RuPC and O_2^- species in a typical Li-O_2 battery environment (Figures 4B-4D and S22). It has been reported that LiO_2 could be solvated by coordination with three DMSO molecules through Li atom to form a solvated complex LiO_2-3DMSO when using DMSO as the electrolyte solvent (Figure 4C).[37] We calculated that the free energy of this complex was -12.7 kcal mol^{-1} (Figure 4B). Notably, the free energy (LiO_2-3DMSO + RuPC) was significantly lowered down to -24.4 kcal mol^{-1} once RuPC was added to the electrolyte (Figure 4B), suggesting that RuPC could interact with the LiO_2 intermediate, which is consistent with the results of UV-vis spectra. Most importantly, a relatively stable, low-reactive complex RuPC(LiO_2-3DMSO) (Figure 4D) was generated by dissociation of the Ru-S coordination bond of RuPC followed by *O*-terminal-coordination of LiO_2-3DMSO to the Ru(II) center. Furthermore, the disproportionation of RuPC(LiO_2-3DMSO) is predicted to be thermodynamically unfavorable whatever the existing form of Li_2O_2. As shown in Table S3, the reaction of 2RuPC(LiO_2-3DMSO) → Li_2O_2 + O_2 + 6DMSO + 2RuPC is strongly endothermic by 61.2 kcal mol^{-1} (entry S1). We expect the Li_2O_2 is not free in the solvent, which could form oligomers; i.e., $(Li_2O_2)_n$. However, even for the n=16 (entry S6), the reaction is still endothermic by 29.7 kcal mol^{-1}. Alternatively, Li_2O_2 could also be stabilized by RuPC. However, DFT calculations showed that the formation of RuPC(Li_2O_2-2DMSO) would not change the unfavorable situation of the disproportionation reaction (entry S7). All these findings lead to the conclusion that forming a RuPC(LiO_2-

3DMSO) complex would not only suppress the side reactions initiated by free LiO_2 but also inhibit the disproportionation reaction. Notwithstanding, the further reduction reaction for RuPC(LiO_2-3DMSO) is still feasible. According to our calculation, the reaction of RuPC(LiO_2-3DMSO) + $Li^+ + e^- \rightarrow Li_2O_2$ + 3DMSO + RuPC is exothermic by 26.6 kcal mol^{-1}.

In order to confirm the existence of RuPC(LiO_2-3DMSO) intermediate during battery operations, we conducted *ex situ* electron paramagnetic resonance (EPR) experiments (Figures 4E, 4F, and S23). As depicted in Figure 4E, the g factor of the KO_2+DMSO solution is around 2.007, which corresponds to the signal of superoxide,[56] and both spectra of the RuPC-containing electrolytes after half discharge and half charge have a similar g factor (g = 2.006). However, in the absence of RuPC, no signals of superoxide appeared for the electrolytes after half discharge or half charge (Figure 4F), which might be due to the instability (short lifetime) of LiO_2 species in $LiClO_4$/DMSO electrolyte without RuPC. Therefore, the EPR signal of RuPC-containing electrolytes after half discharge and half charge can be assigned to the relatively stable RuPC(LiO_2-3DMSO) species, corresponding to the DFT calculations.

Hence, inspired by the experimental and theoretical results, we propose an O_2 redox reaction mechanism for the RuPC-catalyzed Li-O_2 batteries (Figure 5). During the discharge reaction, according to the CV curves (Figure S6A), the RuPC has no reaction features in the discharge voltage region; thus, the first step of the discharge is the one-electron reduction of O_2 to O_2^-, which then quickly combines with Li^+, RuPC, and DMSO, forming a relatively stable, low-reactive intermediate RuPC(LiO_2-3DMSO) (Equation 1) as a result of the interaction between Ru(II) center and O_2^-/LiO_2 intermediates as well as the solvation effect (Figure 4D). Subsequently, as shown by the results of XRD (Figure 3A) and XPS (Figure 3C), the Li_2O_2

species is the main discharge product of the RuPC-catalyzed Li-O_2 batteries. Hence, the RuPC(LiO_2-3DMSO) intermediates would undergo a second reduction (Equation 2) to form Li_2O_2 products. Since the formation of RuPC(LiO_2-3DMSO) is thermodynamically favorable (Figure 4B), the dissolution of LiO_2 in electrolyte can be greatly promoted; thus, introduction of the RuPC electrocatalyst can expand the formation of Li_2O_2 in electrolyte, alleviate the cathode passivation, and increase the discharge capacity, corresponding to the experimental results (Figure 1B). Moreover, compared with the highly reactive O_2^-/LiO_2 intermediates in conventional discharge process, the improved stability and reduced reactivity of the RuPC(LiO_2-3DMSO) intermediate could suppress the superoxide-related side reactions effectively, thus increasing the reversibility (Figures 2E-H) and prolonging the cycle life (Figure 1D). When charging in turn, considering the interaction between RuPC and LiO_2 (Figure 4D), as well as the existence of RuPC(LiO_2-3DMSO) species during the charge process (Figure 4E), the first step of the charge process is the one-electron delithiation of Li_2O_2 to LiO_2 intermediate, which is further converted into the RuPC(LiO_2-3DMSO) intermediate with the assistance of RuPC and DMSO (Equation 3). Later, as shown by the experimental results (Figures 2 and 3), the Li_2O_2 products can be completely removed after charge; thus, a second oxidation (Equation 4) of RuPC(LiO_2-3DMSO) intermediate would be undergone to release the O_2 and regenerate the RuPC to accomplish the overall $2e^-/O_2$ OER process. As the delithiation pathway of Li_2O_2 is more kinetically favorable and highly reversible than the traditional two-electron pathway,[57-59] the RuPC-catalyzed Li-O_2 batteries could effectively reduce the charge overpotential (Figures 1B and 1C).

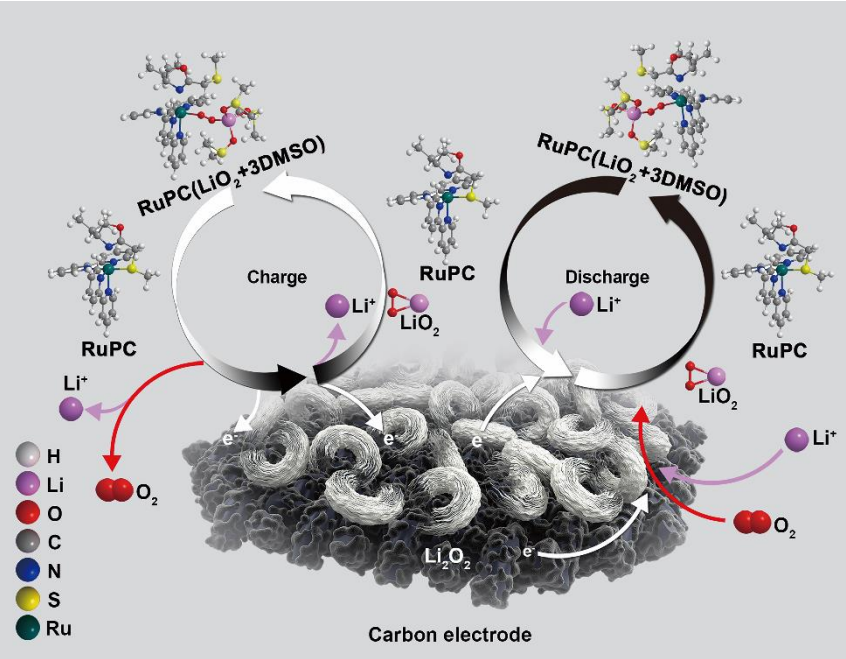

Figure 5. Schematic illustration

Schematic illustration showing the reaction mechanisms of the RuPC-catalyzed Li-O_2 batteries.

ORRs (discharge):

$$O_2(sol) + e^- + Li^+ + 3DMSO + RuPC(sol) \rightarrow RuPC(LiO_2\text{-}3DMSO) \text{ (Equation 1)}$$

$$RuPC(LiO_2\text{-}3DMSO) + e^- + Li^+ \rightarrow Li_2O_2 + 3DMSO + RuPC \text{ (Equation 2)}$$

OERs (charge):

$$Li_2O_2 + 3DMSO + RuPC(sol) \rightarrow RuPC(LiO_2\text{-}3DMSO) + Li^+ + e^- \text{ (Equation 3)}$$

$$RuPC(LiO_2\text{-}3DMSO) \rightarrow O_2 + Li^+ + e^- + 3DMSO + RuPC \text{ (Equation 4)}$$

In summary, we have designed and used an organic-metal complex as a multifunctional soluble catalyst to address the cathode passivation, large polarization, and severe parasitic reactions of current Li-O_2 batteries. Instead of forming the highly reactive O_2^-/LiO_2 intermediates in the conventional discharge process, a relatively stable, low-reactive RuPC(LiO_2-3DMSO) intermediate was formed in the presence of RuPC, which not only limits

the superoxide-related side reactions but also expands the formation of Li_2O_2 in electrolyte during discharge process, thus alleviating the cathode passivation and parasitic reactions significantly. Consequently, the RuPC-catalyzed Li-O_2 batteries exhibited an ultralong cycle life (371 cycles at a current density of 400 mA g^{-1} with a cutoff capacity of 500 mAh g^{-1}) and a high discharge capacity (~9281 mAh g^{-1} at a current density of 200 mA g^{-1}). As for charge process, the initial delithiation of Li_2O_2 with a one-electron process rather than the traditional two-electron mechanism was achieved in the RuPC-catalyzed Li-O_2 batteries, which is more kinetically favorable and highly reversible, leading to a low charge overpotential (0.54 V).

Experimental Procedures

Chemicals and Materials

Unless otherwise mentioned, all chemicals were used directly without further purification after purchase. For more details, see the Supplemental Experimental Procedures.

Synthesis of RuPC

To a solution of (*S*)-4-isopropyl-2-((methylthio)methyl)-4,5-dihydrooxazole (238.5 mg, 1.4 mmol) in ethylene glycol (12.5 mL) was added *cis*-$Ru(bpy)_2Cl_2 \cdot 2H_2O$ (651.1 mg, 1.3 mmol).[41,42] The mixture was heated at 180 ^oC for 20 min under an argon atmosphere and then cooled down to room temperature. An aqueous solution of $NaClO_4$ (1.0 M, 100 mL) was added. The orange precipitate was collected by centrifugation, redissolved in 10 mL of ethanol, and then precipitated by $NaClO_4$ (1.0 M in water, 100 mL). The crude product was purified by flash column chromatography on silica gel (200-300 mesh, eluent with $CH_3CN/H_2O/KNO_3$ (sat.) = 100:3:1). After removal of the solvents, the solid was dissolved in ethanol (5 mL) and

precipitated by $NaClO_4$ (1.0 M in water, 50 mL). The procedure was repeated twice, and after a final wash with water (15 mL x 5), the pure product RuPC was obtained as an orange-red solid (0.85 g, 1.1 mmol, 87% yield, 5:1 diastereoisomers ratio as determined by ^1H NMR).

Li-O_2 battery assembly

The carbon cathode was prepared by coating a homogeneous slurry containing 90 wt % carbon black nanoparticles and 10 wt % polyvinylidene fluoride binders on a carbon cloth supporter and then dried in a vacuum oven at 120 ^oC for 12 hr; the loading of the carbon nanoparticles was about 0.5~1.0 mg cm^{-2}. The electrolyte was prepared by mixing DMSO, $LiClO_4$, and the as-prepared RuPC in the glovebox. The concentrations of the $LiClO_4$ and RuPC were 0.5 M and 0.05 M, respectively. Further, the Li-O_2 battery was assembled with the as-prepared carbon cathode, glass fiber separator, and metallic Li anode into R2032 coin-type Li-O_2 cells using the 0.05 M RuPC-0.5 M $LiClO_4$/DMSO electrolyte. All parts of the cell were dried at 100 ^oC overnight and then assembled in an Ar filled glove box (H_2O < 1 ppm, O_2 < 1 ppm).

Electrochemical Measurements

The batteries were tested in 1 O_2 atmosphere with a NEWARE BTS-5 V/5 mA battery testing system (Shenzhen Neware Elctron, China). The area of the carbon cathode was about 0.8 cm^2. The current densities and battery capacities were calculated based on the basis of the mass of carbon black nanoparticles. The EIS tests were carried out with an impedance analyzer (IM6, Zahner-elektrik, Germany) in a frequency range from 100 kHz to 10 mHz with an amplitude of 5 mV. The CV experiments were tested at an electrochemical workstation (CHI760E, CH Instruments, Shanghai, China) or with an IVIUM multichannel electrochemical analyzer.

Characterizations

The products of discharged and charged electrodes were detected using XRD, recorded on a Rigaku Ultima IV X-ray diffractometer based on Cu Kα radiation (λ=1.5418 Å) with a scan angle range of 10-60^{o}. The nanostructures and surface morphologies of the discharged and charged electrodes were investigated using field emission SEM (HITACHI S-4800). The chemical compositions of the discharged products were characterized using X-Ray Photoelectron Spectroscopy (PHI 5000 Versa Probe III, ULVAC-PHI, Japan). UV-vis absorption spectrometry was performed using a Thermo Evolution 300 spectrophotometer. Flash column chromatography was performed with silica gel (300-400 mesh, pH = 6.7-7.0). ^{1}H NMR and ^{13}C NMR spectra were recorded on a Bruker AM (500 MHz) or Bruker AM (600 MHz) spectrometer at ambient temperature. Infrared spectra were recorded on a Nicolet Avatar 330 FTIR spectrophotometer. High-resolution mass spectra were recorded on a Bruker En Apex Ultra 7.0 T Fourier transform mass spectroscopy instrument using ESI technique. The EPR spectra (-183°C) were recorded on a Bruker EMX-10/12 spectrometer at 9.4 GHz with a modulation frequency of 100 kHz and a modulation amplitude of 2 G.

DFT calculations

In this work, ωB97XD functional theory was carried out. In the ωB97XD calculations, the Ru atom was treated with the Stuttgart-Dresden relativistic effective core potential. For the other atoms, the 6-31G(d,p) basis set was used. In addition, the polarizable continuum model (IEFPCM) was chosen to account for the solvent effect with DMSO solvent, which corresponds to the experimental electrolyte environment. To reduce the overestimation of the entropy contribution of the results, we used a correction of -2.6 (or 2.6) kcal mol^{-1} for 2:1 (or 1:2)

transformations as many earlier theoretical studies did. Natural bond orbital (NBO) analyses were performed using the NBO program as implemented in the Gaussian software packages. All the DFT calculations were carried out with the Gaussian 09 program.

Acknowledgments

This work was supported by the National 973 Program (2015CB251102), the Key Project of National Natural Science Foundation of China (21673196, 21621091, 21703186, 21773192), and the Fundamental Research Funds for the Central Universities (20720150042, 20720150043). The authors thank Prof. Eric Meggers at Philipps-Univeristaet Marburg for his discussion about the synthesis of RuPC complex; Prof. Gang Fu at Xiamen University for his instructive discussions in DFT calculations; Lajia Yu and Dandan Tao at Xiamen University for their assistance in EPR experiments and UV-Vis spectroscopy experiments, respectively; and Yu Gu and Tao Wang at Xiamen University for their discussions in XPS results and CV data, respectively.

Author Contributions

X.L. and R.Y. contributed equally to this work. X.L., R.Y., Q.D., M.Z. and L.G. conceived the project. X.L. and Y.C. designed the electrochemical and characterization experiments, which X.L. then performed. X.L. Y.C., S.C., M.Z. and Q.D. analysed and interpreted the experimental data. R.Y. designed and performed the theoretical calculations. X.L. R.Y., S.C., M.Z. and Q.D. analysed and interpreted the computational data. L.G. and X.D. designed the synthetic route of the ruthenium (II) complex, which X.D. then performed. B.H. performed the NMR, IR, HRMS experiments and analysed the data. Y.H. and Z.Z. performed the DEMS experiments and

analysed the data. X.L. and R.Y. drafted the paper, with support from M.Z. and Q.D., as well as language editing by L.G. All authors discussed the results and commented on the manuscript. The work was supervised by L.G., M.Z. and Q.D.

Declaration of Interests

The authors declare no competing interests.

References and Notes

1. Bruce, P.G., Freunberger, S.A., Hardwick, L.J., and Tarascon, J.-M. (2012). Li-O_2 and Li-S batteries with high energy storage. Nat. Mater. *11*, 19-29.
2. Aurbach, D., McCloskey, B.D., Nazar, L.F., and Bruce, P.G. (2016). Advances in understanding mechanisms underpinning lithium-air batteries. Nat. Energy *1*, 16128.
3. Manthiram, A., Fu, Y., Chung, S.-H., Zu, C., and Su, Y.-S. (2014). Rechargeable Lithium-Sulfur Batteries. Chem. Rev. *114*, 11751-11787.
4. Chang, Z., Xu, J., and Zhang, X. (2017). Recent Progress in Electrocatalyst for Li-O_2 Batteries. Adv. Energy Mater. *7*, 1700875.
5. Li, F., Zhang, T., and Zhou, H. (2013). Challenges of non-aqueous Li-O_2 batteries: electrolytes, catalysts, and anodes. Energy Environ. Sci. *6*, 1125-1141.
6. Luntz, A.C., and McCloskey, B.D. (2014). Nonaqueous Li-Air Batteries: A Status Report. Chem. Rev. *114*, 11721-11750.
7. Lu, J., Li, L., Park, J.-B., Sun, Y.-K., Wu, F., and Amine, K. (2014). Aprotic and Aqueous Li-O_2 Batteries. Chem. Rev. *114*, 5611-5640.
8. Lu, Y.-C., Gallant, B.M., Kwabi, D.G., Harding, J.R., Mitchell, R.R., Whittingham, M.S.,

and Shao-Horn, Y. (2013). Lithium-oxygen batteries: bridging mechanistic understanding and battery performance. Energy Environ. Sci. *6*, 750-768.

9. Black, R., Adams, B., and Nazar, L. (2012). Non-Aqueous and Hybrid Li-O_2 Batteries. Adv. Energy Mater. *2*, 801-815.
10. Lu, Y.-C., Gasteiger, H.A., and Shao-Horn, Y. (2011). Catalytic Activity Trends of Oxygen Reduction Reaction for Nonaqueous Li-Air Batteries. J. Am. Chem. Soc. *133*, 19048-19051.
11. Feng, N., He, P., and Zhou, H. (2016). Critical Challenges in Rechargeable Aprotic Li-O_2 Batteries. Adv. Energy Mater. *6*, 1502303.
12. Lyu, Z., Zhou, Y., Dai, W., Cui, X., Lai, M., Wang, L., Huo, F., Huang, W., Hu, Z., and Chen, W. (2017). Recent advances in understanding of the mechanism and control of Li_2O_2 formation in aprotic Li-O_2 batteries. Chem. Soc. Rev. *46*, 6046-6072.
13. Lin, X., Cao, Y., Cai, S., Fan, J., Li, Y., Wu, Q.-H., Zheng, M., and Dong, Q. (2016). Ruthenium@mesoporous graphene-like carbon: a novel three-dimensional cathode catalyst for lithium-oxygen batteries. J. Mater. Chem. A *4*, 7788-7794.
14. Aetukuri, N.B., McCloskey, B.D., García, J.M., Krupp, L.E., Viswanathan, V., and Luntz, A.C. (2015). Solvating additives drive solution-mediated electrochemistry and enhance toroid growth in non-aqueous Li-O_2 batteries. Nat. Chem. *7*, 50-56.
15. Adams, B.D., Radtke, C., Black, R., Trudeau, M.L., Zaghib, K., and Nazar, L.F. (2013). Current density dependence of peroxide formation in the Li-O_2 battery and its effect on charge. Energy Environ. Sci. *6*, 1772-1778.
16. Sun, D., Shen, Y., Zhang, W., Yu, L., Yi, Z., Yin, W., Wang, D., Huang, Y., Wang, J., Wang, D., et al. (2014). A solution-phase bifunctional catalyst for lithium-oxygen batteries. J. Am.

Chem. Soc. *136*, 8941-8946.

17. Lim, H.-D., Lee, B., Zheng, Y., Hong, J., Kim, J., Gwon, H., Ko, Y., Lee, M., Cho, K., and Kang, K. (2016). Rational design of redox mediators for advanced Li-O_2 batteries. Nat. Energy *1*, 16066.
18. McCloskey, B.D., Speidel, A., Scheffler, R., Miller, D.C., Viswanathan, V., Hummelshøj, J.S., Nørskov, J.K., and Luntz, A.C. (2012). Twin Problems of Interfacial Carbonate Formation in Nonaqueous Li-O_2 Batteries. J. Phys. Chem. Lett. *3*, 997-1001.
19. Ottakam Thotiyl, M.M., Freunberger, S.A., Peng, Z., and Bruce, P.G. (2013). The Carbon Electrode in Nonaqueous Li-O_2 Cells. J. Am. Chem. Soc. *135*, 494-500.
20. Johnson, L., Li, C., Liu, Z., Chen, Y., Freunberger, S.A., Ashok, P.C., Praveen, B.B., Dholakia, K., Tarascon, J.-M., and Bruce, P.G. (2014). The role of LiO_2 solubility in O_2 reduction in aprotic solvents and its consequences for Li-O_2 batteries. Nat. Chem. *6*, 1091-1099.
21. Luntz, A.C., Viswanathan, V., Voss, J., Varley, J.B., Nørskov, J.K., Scheffler, R., and Speidel, A. (2013). Tunneling and Polaron Charge Transport through Li_2O_2 in Li-O_2 Batteries. J. Phys. Chem. Lett. *4*, 3494-3499.
22. McCloskey, B.D., Scheffler, R., Speidel, A., Girishkumar, G., and Luntz, A.C. (2012). On the Mechanism of Nonaqueous Li-O_2 Electrochemistry on C and Its Kinetic Overpotentials: Some Implications for Li-Air Batteries. J. Phys. Chem. C *116*, 23897-23905.
23. Gao, X., Chen, Y., Johnson, L., and Bruce, P.G. (2016). Promoting solution phase discharge in Li-O_2 batteries containing weakly solvating electrolyte solutions. Nat. Mater. *15*, 882-888.

24. Zhang, Y., Wang, L., Zhang, X., Guo, L., Wang, Y., and Peng, Z. (2018). High-Capacity and High-Rate Discharging of a Coenzyme Q_{10}-Catalyzed Li-O_2 Battery. Adv. Mater. *30*, 1705571.

25. Matsuda, S., Kubo, Y., Uosaki, K., and Nakanishi, S. (2017). Potassium Ions Promote Solution-Route Li_2O_2 Formation in the Positive Electrode Reaction of Li-O_2 Batteries. J. Phys. Chem. Lett. *8*, 1142-1146.

26. Gao, X., Jovanov, Z.P., Chen, Y., Johnson, L.R., and Bruce, P.G. (2017). Phenol-Catalyzed Discharge in the Aprotic Lithium-Oxygen Battery. Angew. Chem. *129*, 6639-6643.

27. Xu, J.-J., Chang, Z.-W., Wang, Y., Liu, D.-P., Zhang, Y., and Zhang, X.-B. (2016). Cathode Surface-Induced, Solvation-Mediated, Micrometer-Sized Li_2O_2 Cycling for Li-O_2 Batteries. Adv. Mater. *28*, 9620-9628.

28. Xu, J.-J., Chang, Z.-W., Yin, Y.-B., and Zhang, X.-B. (2017). Nanoengineered Ultralight and Robust All-Metal Cathode for High-Capacity, Stable Lithium-Oxygen Batteries. ACS Cent. Sci. *3*, 598-604.

29. Khetan, A., Luntz, A., and Viswanathan, V. (2015). Trade-Offs in Capacity and Rechargeability in Nonaqueous Li-O_2 Batteries: Solution-Driven Growth versus Nucleophilic Stability. J. Phys. Chem. Lett. *6*, 1254-1259.

30. Lyu, Z., Yang, L., Luan, Y., Renshaw Wang, X., Wang, L., Hu, Z., Lu, J., Xiao, S., Zhang, F., Wang, X., et al. (2017). Effect of oxygen adsorbability on the control of Li_2O_2 growth in Li-O_2 batteries: Implications for cathode catalyst design. Nano Energy *36*, 68-75.

31. Bryantsev, V.S., Giordani, V., Walker, W., Blanco, M., Zecevic, S., Sasaki, K., Uddin, J., Addison, D., and Chase, G.V. (2011). Predicting solvent stability in aprotic electrolyte Li-

air batteries: nucleophilic substitution by the superoxide anion radical ($O_2^{\bullet-}$). J. Phys. Chem. A *115*, 12399-12409.

32. Bryantsev, V.S., and Blanco, M. (2011). Computational study of the mechanisms of superoxide-induced decomposition of organic carbonate-based electrolytes. J. Phys. Chem. Lett. *2*, 379-383.
33. Khetan, A., Pitsch, H., and Viswanathan, V. (2014). Solvent degradation in nonaqueous Li-O_2 batteries: oxidative stability versus H-abstraction. J. Phys. Chem. Lett. *5*, 2419-2424.
34. Freunberger, S.A., Chen, Y., Peng, Z., Griffin, J.M., Hardwick, L.J., Barde, F., Novak, P., and Bruce, P.G. (2011). Reactions in the rechargeable lithium-O_2 battery with alkyl carbonate electrolytes. J. Am. Chem. Soc. *133*, 8040-8047.
35. McCloskey, B.D., Valery, A., Luntz, A.C., Gowda, S.R., Wallraff, G.M., Garcia, J.M., Mori, T., and Krupp, L.E. (2013). Combining Accurate O_2 and Li_2O_2 Assays to Separate Discharge and Charge Stability Limitations in Nonaqueous Li-O_2 Batteries. J. Phys. Chem. Lett. *4*, 2989-2993.
36. Sharon, D., Afri, M., Noked, M., Garsuch, A., Frimer, A.A., and Aurbach, D. (2013). Oxidation of Dimethyl Sulfoxide Solutions by Electrochemical Reduction of Oxygen. J. Phys. Chem. Lett. *4*, 3115-3119.
37. Laoire, C.O., Mukerjee, S., Abraham, K., Plichta, E.J., and Hendrickson, M.A. (2010). Influence of Nonaqueous Solvents on the Electrochemistry of Oxygen in the Rechargeable Lithium-Air Battery. J. Phys. Chem. C *114*, 9178-9186.
38. Seo, J.S., Whang, D., Lee, H., Jun, S.I., Oh, J., Jeon, Y.J., and Kim, K. (2000). A homochiral metal-organic porous material for enantioselective separation and catalysis. Nature *404*,

982-986.

39. Carrettin, S., Corma, A., Iglesias, M., and Sánchez, F. (2005). Stabilization of Au(III) on heterogeneous catalysts and their catalytic similarities with homogeneous Au(III) metal organic complexes. Appl. Catal. A: Gen. *291*, 247-252.
40. Gong, L., Wenzel, M., and Meggers, E. (2013). Chiral-Auxiliary-Mediated Asymmetric Synthesis of Ruthenium Polypyridyl Complexes. Acc. Chem. Res. *46*, 2635-2644.
41. Allen, J.V., Dawson, G.J., Frost, C.G., Williams, I.M.J., and Coote, S.J. (1994). Preparation of novel Sulfur and phosphorus containing oxazolines as ligands for asymmetric catalysis. Tetrahedron *50*, 799-808.
42. Al-Rawashdeh, N.A.F., Chatterjee, S., Krause, J.A., and Connick, W.B. (2014). Ruthenium Bis-diimine Complexes with a Chelating Thioether Ligand: Delineating 1,10-Phenanthrolinyl and 2,2′-Bipyridyl Ligand Substituent Effects. Inorg. Chem. *53*, 294-307.
43. Chen, Y., Freunberger, S.A., Peng, Z., Fontaine, O., and Bruce, P.G. (2013). Charging a Li-O_2 battery using a redox mediator. Nat. Chem. *5*, 489-494.
44. Lim, H.-D., Song, H., Kim, J., Gwon, H., Bae, Y., Park, K.-Y., Hong, J., Kim, H., Kim, T., Kim, Y.H., et al. (2014). Superior Rechargeability and Efficiency of Lithium-Oxygen Batteries: Hierarchical Air Electrode Architecture Combined with a Soluble Catalyst. Angew. Chem. Int. Ed. *53*, 3926-3931.
45. Leroy, S., Martinez, H., Dedryvère, R., Lemordant, D., and Gonbeau, D. (2007). Influence of the lithium salt nature over the surface film formation on a graphite electrode in Li-ion batteries: An XPS study. Appl. Surf. Sci. *253*, 4895-4905.
46. Sivaprakash, S., and Majumder, S.B. (2010). Spectroscopic analyses of

0.5Li[$Ni_{0.8}Co_{0.15}Zr_{0.05}$]$O_2$-0.5Li[$Li_{1/3}Mn_{2/3}$]$O_2$ composite cathodes for lithium rechargeable batteries. Solid State Ionics *181*, 730-739.

47. Yang, Z., Xu, X., Liang, X., Lei, C., Wei, Y., He, P., Lv, B., Ma, H., and Lei, Z. (2016). MIL-53(Fe)-graphene nanocomposites: Efficient visible-light photocatalysts for the selective oxidation of alcohols. Appl. Catal. B: Environ. *198*, 112-123.
48. Ryu, W.-H., Gittleson, F.S., Thomsen, J.M., Li, J., Schwab, M.J., Brudvig, G.W., and Taylor, A.D. (2016). Heme biomolecule as redox mediator and oxygen shuttle for efficient charging of lithium-oxygen batteries. Nat. Commun. *7*, 12925.
49. Gu, Y., Wang, W.-W., Li, Y.-J., Wu, Q.-H., Tang, S., Yan, J.-W., Zheng, M.-S., Wu, D.-Y., Fan, C.-H., Hu, W.-Q., et al. (2018). Designable ultra-smooth ultra-thin solid-electrolyte interphases of three alkali metal anodes. Nat. Commun. *9*, 1339.
50. Li, N.-W., Yin, Y.-X., Yang, C.-P., and Guo, Y.-G. (2015). An Artificial Solid Electrolyte Interphase Layer for Stable Lithium Metal Anodes. Adv. Mater. *28*, 1853-1858.
51. Liang, X., Hart, C., Pang, Q., Garsuch, A., Weiss, T., and Nazar, L.F. (2015). A highly efficient polysulfide mediator for lithium-sulfur batteries. Nat. Commun. *6*, 5682.
52. Li, Y.-J., Fan, J.-M., Zheng, M.-S., and Dong, Q.-F. (2016). A novel synergistic composite with multi-functional effects for high-performance Li-S batteries. Energy Environ. Sci. *9*, 1998-2004.
53. Park, M.-S., Lim, Y.-G., Park, J.-W., Kim, J.-S., Lee, J.-W., Kim, J.H., Dou, S.X., and Kim, Y.-J. (2013). Li_2RuO_3 as an Additive for High-Energy Lithium-Ion Capacitors. J. Phys. Chem. C *117*, 11471-11478.
54. Sathiya, M., Ramesha, K., Rousse, G., Foix, D., Gonbeau, D., Prakash, A.S., Doublet, M.L.,

Hemalatha, K., and Tarascon, J.M. (2013). High Performance $Li_2Ru_{1-y}MnyO_3$ ($0.2 \leq y \leq 0.8$) Cathode Materials for Rechargeable Lithium-Ion Batteries: Their Understanding. Chem. Mater. *25*, 1121-1131.

55. Staniewicz, R.J., Sympson, R.F., and Hendricker, D.G. (1977). Preparation and investigation of the spectral and electrochemical properties of mixed-ligand ruthenium (II) complexes containing 1, 8-naphthyridines. Inorg. Chem. *16*, 2166-2171.
56. Lindsay, D., and Garland, D. (1987). ESR spectra of matrix-isolated lithium superoxide. J. Phys. Chem. *91*, 6158-6161.
57. Xie, J., Dong, Q., Madden, I., Yao, X., Cheng, Q., Dornath, P., Fan, W., and Wang, D. (2015). Achieving Low Overpotential Li-O_2 Battery Operations by Li_2O_2 Decomposition through One-Electron Processes. Nano Lett. *15*, 8371-8376.
58. Lu, Y.-C., and Shao-Horn, Y. (2013). Probing the Reaction Kinetics of the Charge Reactions of Nonaqueous Li-O_2 Batteries. J. Phys. Chem. Lett. *4*, 93-99.
59. Kang, S., Mo, Y., Ong, S.P., and Ceder, G. (2013). A facile mechanism for recharging Li_2O_2 in Li-O_2 batteries. Chem. Mater. *25*, 3328-3336.